MULTIPLE SOLUTIONS OF THE TRANSONIC POTENTIAL FLOW EQUATION

81-1019

John Steinhoff* and Antony Jameson**
Grumman Aerospace Corporation
Bethpage, New York 11714

Abstract

The two-dimensional transonic potential flow equation, when solved in discrete form for steady flow over an airfoil, has been found to yield more than one solution in certain bands of angle of attack and Mach number. The most striking example of this is the appearance of nonsymmetric solutions with large positive or negative lift, for symmetric airfoils at zero angle of attack. The behavior of these "anomalous" solutions is examined as grid size is varied by large factors and found to be not qualitatively different from that of "normal" solutions (outside the nonuniqueness band). Thus it appears that the effect is not due to discretization error, and that the basic transonic potential flow partial differential equation admits nonunique solutions for certain values of angle of attack and Mach number.

Introduction

The full potential equation is widely used for computing transonic flow over aircraft. It expresses conservation of mass, neglecting effects due to viscosity, vorticity and entropy production. For flow without massive separated regions, where the shocks are not too strong, the equation is a good approximation to the Navier-Stokes equations outside of a thin boundary layer and wake region. In combination with boundary layer methods, it has been used to give very accurate solutions for flow over airfoils in two dimensions.[1]

Recently, the authors discovered that in certain bands of angle of attack and Mach number, the full potential equation, when solved in discrete form for steady flow over airfoils, yields multiple solutions. These solutions have very different values of lift and drag. Preliminary results appear in Ref (2).

The purpose of this paper is to present results of numerical experiments designed to test whether the non-uniqueness appears as a result of the discretization procedure, or whether the continuum problem admits a corresponding nonuniqueness. Even if these solutions are caused by discretization error, it may be important to know that a small perturbation can result in a very different solution.

The paper consists of three basic parts. In the first, details of the difference scheme are described. In the second, results are presented for a symmetric Joukowski airfoil at zero angle of attack (α) and fixed free-stream Mach number (M_∞). Here, in addition to the expected symmetric solution, two (mirror-image) unsymmetric solutions appear with large absolute value of lift coefficient (C_L). In this section we attempt to validate these solutions by checking that boundary conditions and the Kutta condition are satisfied, and by studying the variation of the solutions as the computational grid and artificial viscosity are varied. In the third part, the behavior of the "anomalous" solutions is studied as M_∞ and α are varied.

Difference Scheme

In a curvilinear coordinate system, the full potential equation can be written[3]

$$\frac{\partial}{\partial X}(\rho h U) + \frac{\partial}{\partial Y}(\rho h V) = 0$$

where

$$h = \det(H) \ .$$

The isentropic relation for the density

$$\rho = \left[1 + \frac{\gamma - 1}{2} M_\infty^2 (1 - q^2)\right]^{1/(\gamma-1)}$$

where q is the speed and γ is the ratio of specific heats. The basic transformation from physical (x, y) to computational (X, Y) frames is expressed by the matrix

$$H = \begin{pmatrix} x_X & x_Y \\ y_X & y_Y \end{pmatrix} .$$

The physical velocities are derived from a potential, ϕ

$$\begin{pmatrix} u \\ v \end{pmatrix} = (H^\dagger) \begin{pmatrix} \phi_X \\ \phi_Y \end{pmatrix} + \begin{pmatrix} u_\infty \\ v_\infty \end{pmatrix}$$

and the contravariant velocities required for the transformed flux balance equation are

$$\begin{pmatrix} U \\ V \end{pmatrix} = (H)^{-1} \begin{pmatrix} u \\ v \end{pmatrix} .$$

*Staff Scientist, Research Department
**Professor, Dept. of Mechanical and Aerospace Engineering, Princeton University

We use the "finite volume" discretization scheme described in Ref (3). Here, two interlocking meshes are used. On one, the potential ϕ and the coordinates (x,y, X,Y) are defined and the flux balance is satisfied (at convergence). On the other, which coincides with the cell centers of the first, the density and velocities are defined.

Except for one case computed with a parabolic mapping, all of our calculations use an "O" type grid. A Joukowski transformation is used to map the airfoil to a near circle which is then mapped to a circle by a shearing transformation (for a Joukowski airfoil this shearing is not needed).

A stretching and inversion are then used

$$R' = [\Delta + (1-\Delta)R]^{-1}$$

where R' is the radius of a point in the initial mapped plane, R is the radius in the computational plane, and Δ is a small parameter which controls the far field boundary.

The compressible vortex solution

$$\phi_F = \frac{\Gamma}{2\pi} \tan^{-1}(\beta \tan\theta), \qquad (1)$$

$$\beta = (1 - M_\infty^2)^{1/2},$$

is used for the far field boundary conditions, where Γ is the value of the circulation. The requirement that there be no flow around the trailing edge determines Γ.

The calculation of the supersonic zone is stabilized by the addition of artificial viscosity to provide an upwind bias. This has the form

$$P_{i+\frac{1}{2},j} - P_{i-\frac{1}{2},j} + Q_{i,j+\frac{1}{2}} - Q_{i,j-\frac{1}{2}}$$

where P and Q are defined as follows.

A switching function is defined:

$$\mu = \max(0, 1 - M_c^2/M^2).$$

This vanishes when the local Mach number, M, is less than a cutoff, M_c.

Also, let

$$\tilde{P} = \rho h \frac{\mu}{a^2} \left(U^2 \frac{\partial^2}{\partial X^2} + UV \frac{\partial^2}{\partial X \partial Y} \right) \phi$$

$$\tilde{Q} = \rho h \frac{\mu}{a^2} \left(UV \frac{\partial^2}{\partial X \partial Y} + V^2 \frac{\partial^2}{\partial Y^2} \right) \phi .$$

Then

$$P_{i+\frac{1}{2},j} = \tilde{P}_{i,j} - \epsilon_{ij} \tilde{P}_{i-1,j} \qquad (U > 0)$$

$$P_{i+\frac{1}{2},j} = \epsilon_{i+1,j} \tilde{P}_{i+2,j} - \tilde{P}_{i+1,j} \quad (U < 0)$$

with corresponding formulas for $Q_{i,\, j+\frac{1}{2}}$.

If the coefficient $\epsilon = 1 - 0(\Delta X)$, then $P = 0(\Delta X)$ and the added terms are $0(\Delta X^2)$, since the difference in P is not divided by ΔX. Accordingly this coefficient is defined

$$\epsilon_{i,j} = \max(0, 1 - \lambda(\rho_{i+\frac{1}{2},j} - \rho_{i-\frac{1}{2},j})).$$

The density difference acts as a shock detector, causing the scheme to revert to a first order accurate form near a shock wave. In the calculations presented in this paper, the artificial viscosity is cut off at Mach number, $M_c \sim .8$.

A multigrid - approximate factorization scheme (4) is used to solve the discrete equations. This provides strong damping for error components in all frequency bands and allows us to converge to machine accuracy, if desired. The far field boundary conditions are updated to allow for changes of circulation after each iteration on each grid.

Multiple Solutions

Figures 1 and 2 show the pressure distribution (C_p) over the upper and lower surfaces for two alternative solutions of the flow past an 11.8% thick Joukowski airfoil at a Mach number of .832 and zero angle of attack. One solution is symmetric, as expected. The other is unsymmetric, with the shock wave on the upper surface displaced rearward to a point near but not at the trailing edge, and the shock wave on the lower surface displaced forward. The lift coefficient, C_L, is +.5544 for this unsymmetric solution and there is a corresponding mirror image solution with a lift coefficient of -.5544. The grid for these calculations was an "O" mesh, depicted in Fig. 3, with 256 cells around the airfoil and 64 cells between the airfoil and the outer boundary.

The first test made on the "anomolous" solutions was that they accurately satisfy the difference equations. The decay of the average residual for this grid and a similar solution on a 128 x 32 grid is plotted in Fig. 4. The multigrid scheme allows us to converge to machine accuracy, if desired, and there is no doubt that the difference equations are satisfied. Tests were made to verify that the same code would converge to either the + C_L, the - C_L or the symmetric solution is started close enough to each.

The next check was to verify that the far field boundary conditions are properly satisfied. With the free stream subtracted out, these are Dirichlet conditions corresponding to a compressible vortex (eq. 1). The computed solution was found to decay smoothly in the far field like a vortex and doublet in a uniform stream at zero angle of attack, exactly as expected. As a further check, the distance to the outer boundary was reduced from 25 chords to 8 chords by reducing the grid stretching. This caused only a 5% change (increase) in the lift coefficient.

Another check on these solutions concerned the Kutta condition. The pressures on the upper and lower surfaces smoothly went to the same value at the trailing edge and the streamline left the trailing edge smoothly.

The final test was to verify the convergence of the solution with grid refinement. In Fig. 5, values of C_L are plotted for the unsymmetric solu-

tion on grids with 96 x 24, 128 x 32, 192 x 48, 256 x 64 and 384 x 192 cells. For comparison, C_L is also plotted for the same airfoil at $M_\infty = .75$, $\alpha = 2°$, where only one solution was found. It can be seen that C_L converges at comparable rates for the two solutions. The reason that C_L decreased as the grid was refined for the $\alpha = 0$ solution was that the lower shock, which was weaker than the upper one, became stronger and moved backward, increasing the magnitude of the negative contribution of the lower part of the airfoil to C_L. The upper shock did not change as much as the grid was refined. For the $\alpha = 2°$ case, there was only a single shock located at the upper surface, which moved backward as the grid was refined.

The artificial viscosity in these calculations had the second order form defined in the previous section. It was verified that the unsymmetric solutions could also be obtained with the first order accurate form of artificial viscosity obtained by setting $\varepsilon = 0$.

In order to check whether the solution is a peculiarity depending on the form of the grid, calculations were also performed on a "C" mesh generated by mapping to parabolic coordinates. The solution is displayed in Fig. 6 for a grid with 128 x 32 cells. With this type of mesh, the cell width near the trailing edge was 400 times the width on the 256 x 64 "O" mesh. It can be seen that the unsymmetric solution persists.

Hysteresis

The unsymmetric solutions have been found only in a narrow Mach number band. In the case of the 11.8% thick Joukowski airfoil at zero angle of attack, only the symmetric solution could be found below .82 and above .85. The lift coefficient for the unsymmetric solution at $\alpha = 0$ is plotted in Fig. 7 for Mach numbers between these limits. In this band the non-uniqueness was associated with a hysteresis. In Fig. 8, C_L as a function of α is plotted for a series of Mach numbers. The curves for Mach number less than .82 show the expected behavior. Above .82, on the other hand, we find the hysteresis. On the .832 Mach number curve, the two intercepts of the C_L axis at $\alpha = 0$ correspond to the two unsymmetric solutions discussed in the previous section. Starting from the upper right hand part of this curve, which corresponds to the upper shock being close to the trailing edge, we can generate the rest of the curve by incrementally decreasing α and, at each step, computing a new solution from the previous one. Once we decrease α below about -.14° the solution "flips" to the negative C_L one. We can then generate this part of the curve in the same way. The symmetric solution ($C_L = 0$, $\alpha = 0$) proved to be unstable to small perturbations, and went over to either the positive or negative C_L ($\alpha = 0$) solution.

Below the Mach number where hysteresis appears, it can be seen that the change in C_L for a small change in α at $\alpha = 0$ increases as we increase M_∞ and becomes large as we approach a critical value, M_{crit}.

Thinking of α as a function of C_L, we see that the slope of α vs. C_L at $C_L = 0$ goes smoothly to zero at M_{crit}, and there is the possibility that it can become negative beyond M_{crit}, where the hysteresis is found.

The hysteresis occurs in a rather narrow band of angle of attack. If this band were to become smaller as the mesh was refined, there is a possibility that instead of a non-unique solution there would be a rapid switch from large negative to large positive C_L as the angle of attack passed through zero. Refinement of the mesh did not indicate any significant narrowing of the band, however. Its width was also insensitive to the far field stretching and placement of the outer boundary. Also, the value of M_{crit} was not sensitive to mesh refinement or far field stretching.

A final result is presented in Fig. 9. Values of C_L vs. α for an RAE 2822 airfoil at .725 Mach number were computed using a "C" mesh with the first order form of artificial viscosity. A similar hysteresis band can be seen. Similar results have also been found for an NYU 82-06-09 airfoil. Here, a conservative finite difference rather than finite volume scheme was used (details of this scheme are presented in Ref. 5).

Conclusions

Multiple solutions of the discrete full potential equation have been found for steady two dimensional flow over airfoils. The most striking example is the appearance of unsymmetric solutions with large positive or negative values of lift for a symmetric airfoil at zero angle of attack. This occurs only in a narrow band of Mach number, between .82 and .85 in the case of an 11.8% thick Joukowski airfoil.

Extensive numerical experiments, including the use of alternative grids and extreme grid refinement, have confirmed the persistence of these solutions. Hence, it appears likely that they actually correspond to a non-uniqueness of the continuum problem, and are not a consequence of discretization error. Since the rearward shock wave in the unsymmetric solution is not quite at the trailing edge, it seems that the non-uniqueness is not caused by interference between a shock wave at the trailing edge and the Kutta condition.

The multiple solutions may have a physical counterpart. The Mach number band in which they appear is just the band in which an airfoil of this thickness typically experiences buffeting, with the upper and lower shocks alternately reaching a forward and rearward position similar to our positive and negative lift solutions. While buffeting may be triggered by boundary layer separation, this raises the question of whether an instability of the outer inviscid part of the flow may also be a contributing factor to this phenomenon.

The non-unique solutions were found by a sophisticated iterative method, and it is not known whether they correspond to stable equilibrium points of the true time dependent equation. Also, it is not known whether they are only associated with the potential flow approximation, or whether a similar non-uniqueness can also occur in solutions to the Euler or Navier Stokes equations. An investigation of these

questions would shed more light on the possible physical significance of this phenomenon.

References

1. Melnik, R.W., Chow, R., and Mead, H.R., "Theory of Viscous Transonic Flow over Airfoils at High Reynolds Number," AIAA Paper 7-680, 1977.

2. Steinhoff, J.S. and Jameson, A., "Non-Uniqueness in Transonic Potential Flows," Proc. of GAMM Specialist Workshop for Numerical Methods in Fluid Mechanics, Stockholm, September 1979.

3. Jameson, A. and Caughey, D.A., "A Finite-Volume Method for Transonic Potential Flow Calculations," Proc. of AIAA 3rd Computational Fluid Dynamics Conference, pp. 35-54, Albuquerque, N.M., June 27-29, 1977.

4. Jameson, A., "A Multi-Grid Scheme for Transonic Potential Calculations on Arbitrary Grids," Proc. of AIAA 4th Computational Fluid Dynamics Conference, pp. 122-146, Williamsburg, Va., July 23-25, 1979.

5. Bauer, F., Garabedian, P., Korn, D., and Jameson, A., "Supercritical Wing Sections II," Springer Verlag, New York, 1975.

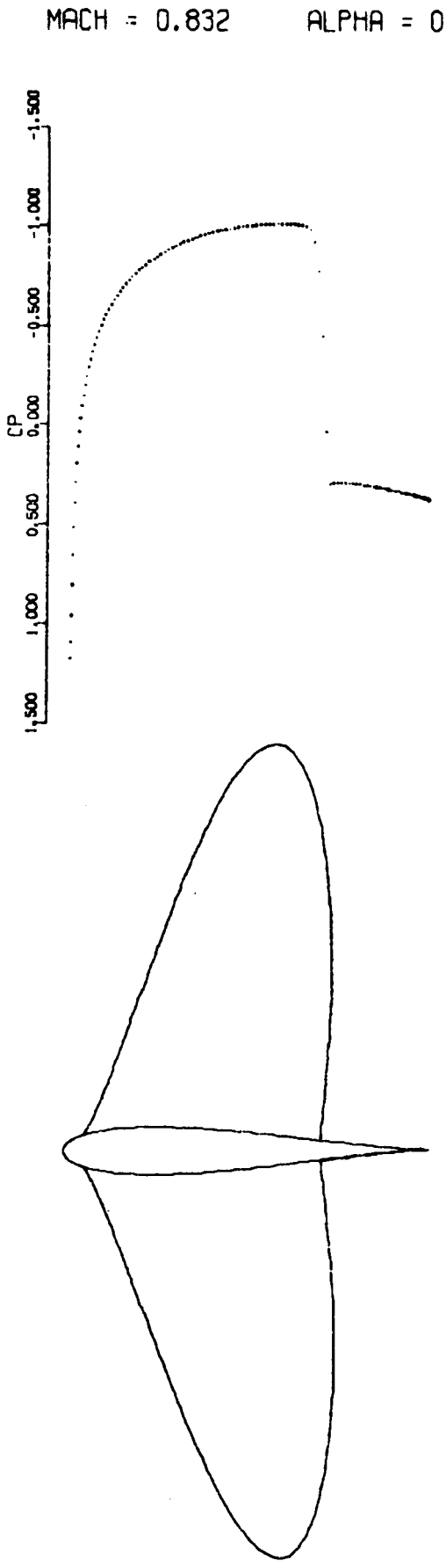

Fig. 1 Symmetric Solution

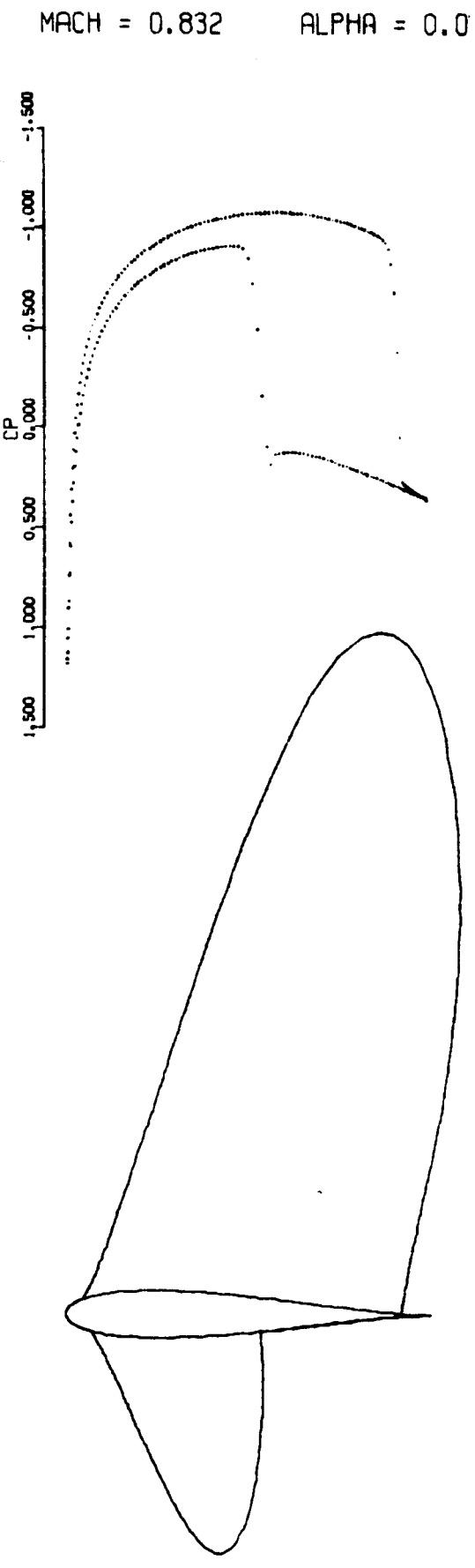

Fig. 2 Unsymmetric Solution

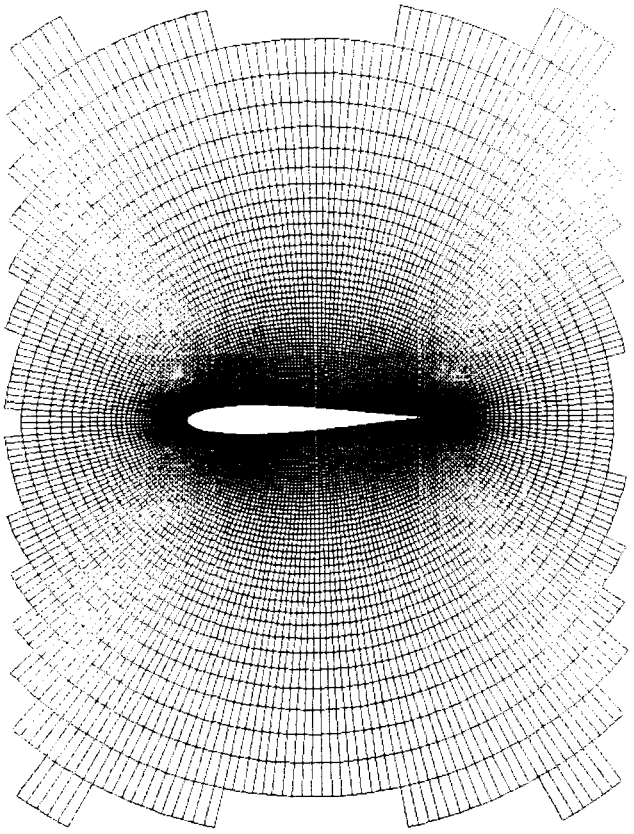

Fig. 3 Computational Grid

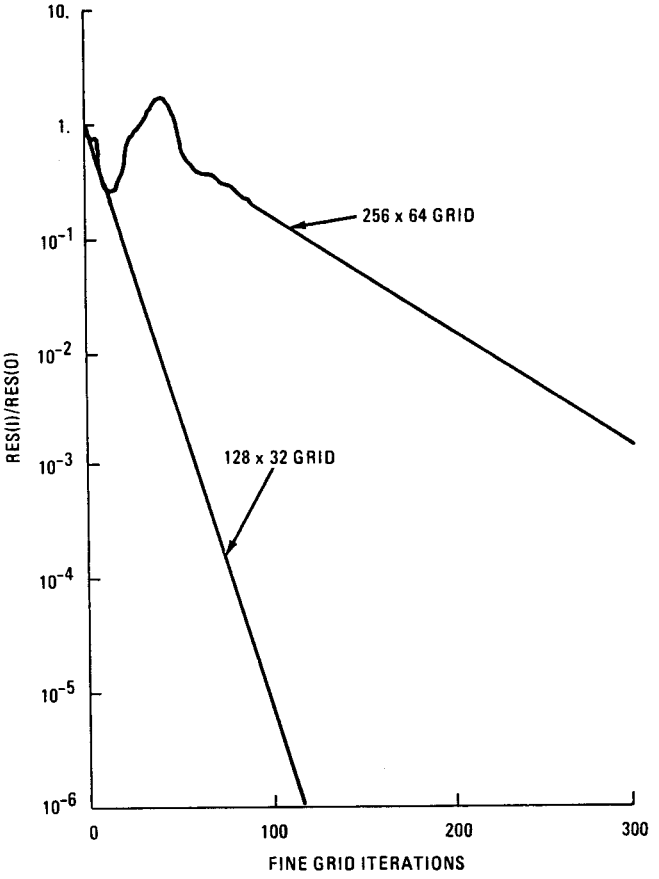

Fig. 4 Residual Decay

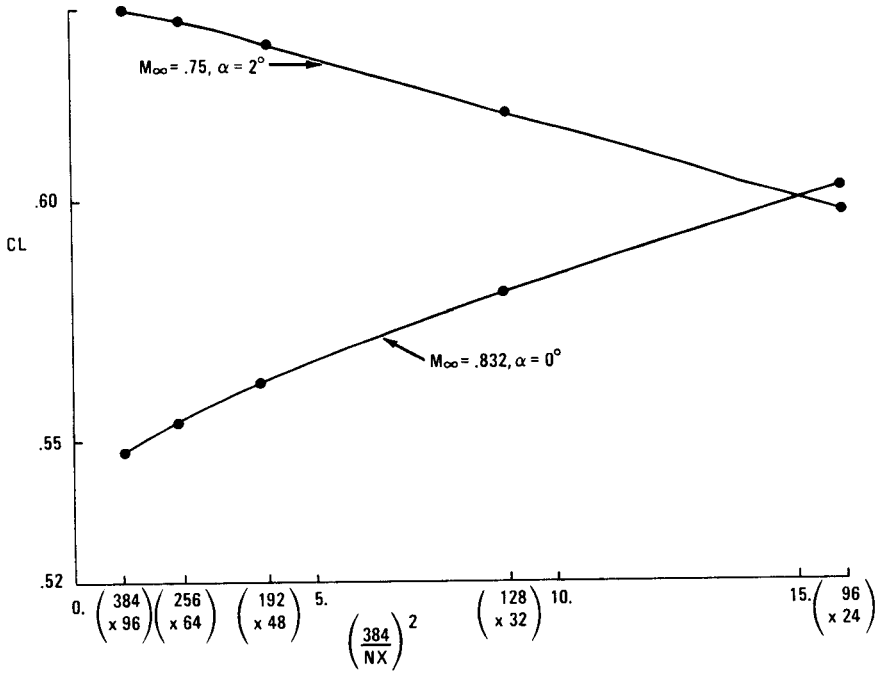

Fig. 5 Lift Convergence

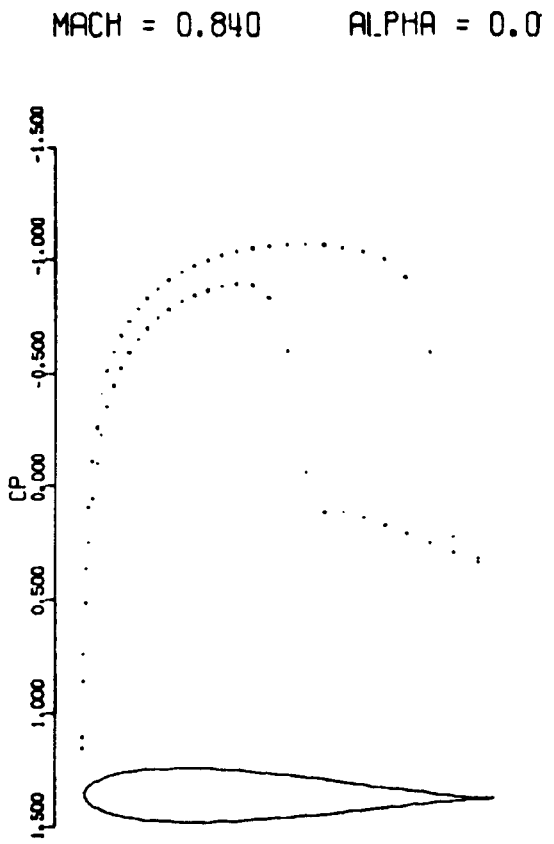

Fig. 6 Unsymmetric Solution
Parabolic Coordinates

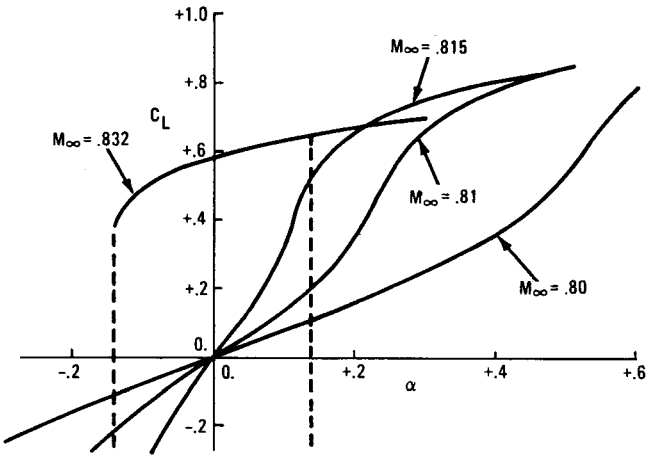

Fig. 7 Hysteresis

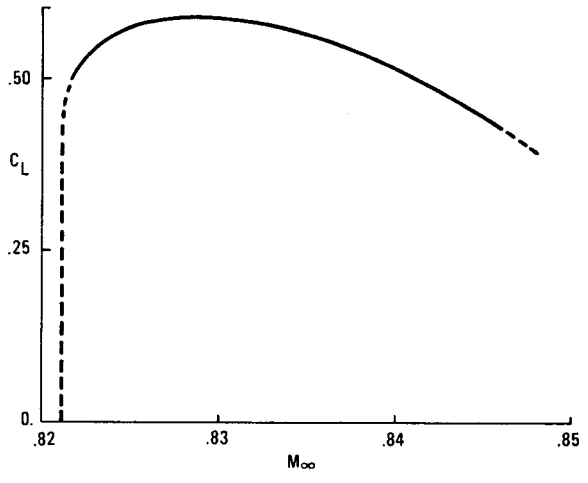

Fig. 8 Unsymmetric Solution
$\alpha = 0.$

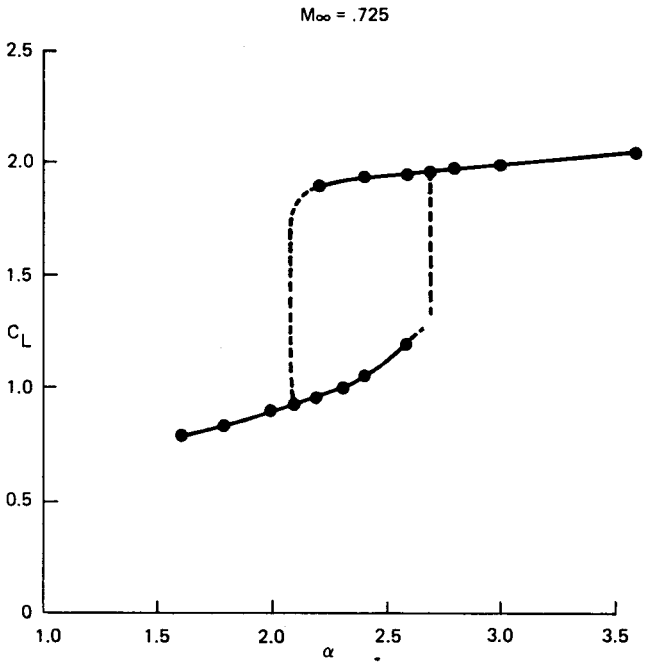

Fig. 9 Hysteresis RAE 2822
Airfoil